Eur. Phys. J. B **23**, 297–305 (2001)

THE EUROPEAN PHYSICAL JOURNAL B

EDP Sciences

The role of layer-thickness deviation in dispersion and structure of plasmons in finite superlattices

M.A. Gilmore and B.L. Johnson[a]

Department of Physics and Astronomy, Western Washington University, Bellingham, 98225, Washington, USA

Received 16 April 2001 and Received in final form 6 July 2001

Abstract. We study the effects of layer thickness variations on the collective plasmon excitation modes of finite superlattices. Unlike other symmetry lowering mechanisms, thickness variation does not strongly localize the surface modes. We find that the reason for this insensitivity lies in the fact that the collective modes of a given finite structure must evolve continuously from the single-finite-superlattice at zero thickness deviation into modes of a pair of uncoupled finite structures at large thickness variation. We also show that this behavior is analogous to the evolution of molecular orbitals from atomic orbitals as the internuclear separation is reduced, in contrast to the analogy of the superlattice modes as a stack of coupled quantum wells. This emphasizes the difference between the *electromagnetic* symmetry of the finite superlattice and the structural symmetry.

PACS. 73.21.-b Electron states and collective excitations in multilayers, quantum wells, mesoscopic, and nanoscale systems – 73.21.Cd Superlattices

1 Introduction

Superlattices, or artificially layered structures, have been the focus of much attention for nearly three decades. Many theoretical and experimental studies have been done, on a range of different phenomena, often focusing on the behavior of collective effects. Such work includes studies of magnons [1–4], phonons [5–8], polaritons [9–11], and plasmons [12–17,21,22]. In particular, surface waves, *i.e.* collective excitations of the finite or semi-infinite superlattice which are localized to the outer boundaries, show many unique and interesting properties. In semi-infinite structures, the existence of the surface wave depends upon the ratio of layer thickness within a unit cell [16]. In addition, in finite structures, the surface waves may be dramatically localized to a single surface by small perturbations of system parameters, or the surface waves may be nonreciprocal, *i.e.* the frequency (energy) of the mode may depend upon the propagation direction [10,23].

It is reasonable to ask about the effect of thickness variation on the collective plasma oscillations of the structure, since real structures will contain some thickness variation. Interestingly, it has been demonstrated that perturbations in the thickness of the constituent layers of the superlattice have little effect on the collective plasmon surface waves in finite structures [24]. This result is surprising for two reasons. The tremendous sensitivity of the surface modes to the overall symmetry, as demonstrated by previous work regarding the effects of dielectric perturbations, would lead one to inquire about the lowering of the periodic symmetry of the structure *via* thickness variation. In addition, work on coupled quantum wells indicates that the electronic wave function of the overall structure is dramatically localized by thickness variation [17].

In this paper, we study the reasons for the insensitivity of the modes to thickness variation, the interesting effects of coupling finite superlattices, and investigate an interesting parallel between the problem of coupled finite superlattices and the evolution of separate atomic orbitals into molecular orbitals. This is the principal insight of the paper – that the thickness perturbation must be viewed as part of the evolution of a larger system, in contrast to the symmetry-lowering of a single structure; the single-structure arguments work well for symmetries based upon the electromagnetic properties of the system, but must be abandoned for this structural perturbation. In particular, we find that the dispersion relations (the allowed plasmon frequencies as a function of wavevector) of finite superlattices with a thickness variation in one layer are insensitive to small variations because the modes *must evolve continuously* into those of two uncoupled structures when the thickness variation gets very large. The parallels to the molecular orbital case (as opposed to the single-structure coupled quantum wells case) are as follows: the allowed plasmon frequencies for two identical finite superlattices split when the two superlattices are coupled, in analogy with the splitting of atomic orbital energies when the atoms are coupled. The splitting of the plasmon frequencies is roughly inversely proportional to the separation. Furthermore, the potential profiles of the split plasmon modes assume an odd-even parity, similar to "bonding/anti-bonding" pairs in the molecular orbital

[a] e-mail: bljohnso@physics.wwu.edu

case. We demonstrate these effects for two identical finite superlattices as well as for small "split-off" structures.

In order to isolate the effects of the symmetry-lowering, we study plasmons in the long-wavelength, quasi-static approximation, using simple model dielectric functions, and ignore the effects of retardation and higher order many-body correlations. Although these effects are important [14,15,18–20], our results are based upon the overall symmetry of the collective superlattice modes composed of long-wavelength static surface modes supported by the individual free-charge layers. An isolated slab will support both bulk and surface excitations; however, by keeping only the static approximation (*i.e.* Laplace's equation) and not enforcing conditions on the dielectric function (*i.e.* looking for the dielectric function to vanish as functions of retardation or correlation parameters), we have a simple and plausible system for which the structural symmetry effects may be elucidated. The structure of the the simple plasmons studied here is well-known: the bulk modes are in two bands, an acoustic branch with linear dispersion at small wavenumber and an optical branch which approaches the plasma frequency at small wavenumber, with surface modes at particular energies that depend upon the layer thicknesses. It can be shown [16] that the surface modes do not exist when the free-charge layer thickness is less than the dielectric layer thickness. In addition, the effect of correlations (as well as tunneling) between active layers becomes important when the spacer layer becomes thin (with respect to the Wigner-Seitz radius), and gaps will appear in the plasmon spectrum [14,18]. In addition, retardation effects will produce shear modes [15] in the low-frequency dispersion, and the retardation and the correlations both provide a general broadening of mode frequencies of the spectral features. In this paper, we will restrict the analysis to layer thicknesses where the surface modes always exist, and where the interlayer coupling may be treated *via* simple classical Coulomb coupling; finally, in the interest of clarity, we will ignore damping and any retardation.

The remainder of this paper is organized as follows. In Section 2 we present the method used for finding the implicit dispersion relation for the finite superlattice. In Section 3 we present some numerical examples of the previous theory, showing the dispersion curves for a finite superlattice and the potential profiles of some of the existing modes. In Section 4 we explore perturbations in layer thickness, creating coupled finite superlattices, and consider the comparison with atomic-to-molecular orbital evolution. Finally, in Section 5 we summarize our results.

2 Theory

This section will lay the theoretical development for calculating the plasmon dispersion for the superlattice, as well as the method for calculating the electrostatic potential of the plasmon modes as a function of depth in structure. We will write out the potential in each region of the superlattice explicitly in order to have the ability to create thickness variations between layers. The use of other methods, *i.e.* the finite-structure dispersion defined by Johnson *et al.* [17] would not leave us this freedom. Consider the superlattice to be a finite number N of alternating layers of materials A and B surrounded by vacuum. Take layers A to have a dielectric constant $\epsilon_{\mathrm{A}}(\omega)$ and layers B to have $\epsilon_{\mathrm{B}}(\omega)$. To begin with, all material A layers will be of thickness d_1 and all the B layers d_2. Later in the paper this condition will be relaxed, and the effect of thickness deviations on the allowed modes will be studied in detail. We orient the superlattice with the z-axis normal to the interfaces and the x-axis parallel to the same (see Fig. 1).

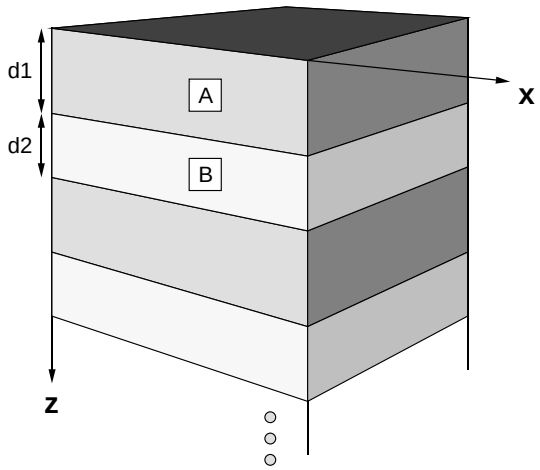

Fig. 1. Physical picture of the superlattice with alternating materials A and B of thicknesses d_1 and d_2, respectively. The z-axis is oriented normal to all the interfaces and the x-axis parallel.

We consider collective electromagnetic excitations of the superlattice which generate a macroscopic electric field. These are coupled excitations of the individual layers; a time-varying electric field in one layer couples to the charges in adjacent layers *via* the Coulomb interaction. The fields can be described *via* a scalar potential in the long-wavelength quasi-static approximation (wherein the curl of the electric field vanishes). The scalar potential, $\phi(\mathbf{x},t)$, must obey Laplace's equation

$$\nabla^2\phi(\mathbf{x},t)=0 \tag{1}$$

everywhere inside and outside the superlattice. The potential will have some translationally invariant profile $\Phi(z)$ and some wave vector $\mathbf{k}$, defined along the x-axis (with no loss of generality). The potential then has the form

$$\phi(\mathbf{x},t)=\Phi(z)\mathrm{e}^{\mathrm{i}(kx-\omega t)}. \tag{2}$$

Applying equation (1) yields

$$\left[\frac{\mathrm{d}^2}{\mathrm{d}z^2}-k^2\right]\Phi(z)=0 \tag{3}$$

with the general solution being decaying exponentials from the outside boundaries of the superlattice and linear combinations of increasing and decreasing exponentials within the layers, *i.e.*

$$\Phi(z)=A_0\mathrm{e}^{kz}; \qquad z<0; \tag{4}$$

while within the superlattice layers,

$$\Phi(z) = A_{2i-1}\mathrm{e}^{kz} + A_{2i}\mathrm{e}^{-kz} \tag{5}$$

where A_{2i-1} and A_{2i} designate the ith layer's coefficients. Finally, below the superlattice, represented as the $N+1$ layer,

$$\Phi(z) = A_{2N+1}\mathrm{e}^{-kz}; \qquad z > \frac{N}{2}(d_1 + d_2). \tag{6}$$

Next we require that $\Phi(z)$ be continuous at each interface along with the normal component of the displacement field $D_z = \epsilon(\omega)\frac{\mathrm{d}\Phi}{\mathrm{d}z}$. For the continuity of $\Phi(z)$,

$$A_0 = A_1 + A_2 \tag{7}$$

$$A_1\mathrm{e}^{kd_1} + A_2\mathrm{e}^{-kd_1} = A_3 + A_4 \tag{8}$$

$$A_3\mathrm{e}^{kd_2} + A_4\mathrm{e}^{-kd_2} = A_5 + A_6 \tag{9}$$

and so on, until the boundary after the Nth layer gives

$$A_{2N-1}\mathrm{e}^{kd_2} + A_{2N}\mathrm{e}^{-kd_2} = A_{2N+1}. \tag{10}$$

For the continuity of the normal component of the displacement, with vacuum outside ($\epsilon_{\mathrm{outside}} = 1$),

$$A_0 = \epsilon_{\mathrm{A}}(\omega)A_1 - \epsilon_{\mathrm{A}}(\omega)A_2 \tag{11}$$

$$\epsilon_{\mathrm{A}}(\omega)A_1\mathrm{e}^{kd_1} - \epsilon_{\mathrm{A}}(\omega)A_2\mathrm{e}^{-kd_1} = \epsilon_{\mathrm{B}}(\omega)A_3 - \epsilon_{\mathrm{B}}(\omega)A_4 \tag{12}$$

$$\epsilon_{\mathrm{B}}(\omega)A_3\mathrm{e}^{kd_2} - \epsilon_{\mathrm{B}}(\omega)A_4\mathrm{e}^{-kd_2} = \epsilon_{\mathrm{A}}(\omega)A_5 - \epsilon_{\mathrm{A}}(\omega)A_6 \tag{13}$$

and so on, until

$$\epsilon_{\mathrm{B}}(\omega)A_{2N-1}\mathrm{e}^{kd_2} - \epsilon_{\mathrm{B}}(\omega)A_{2N}\mathrm{e}^{-kd_2} = -A_{2N+1}. \tag{14}$$

The result is a set of $2N+2$ equations which describe the unknown amplitudes. We translate these into matrix form and then require the determinant of the coefficient matrix to vanish, providing an implicit dispersion relation.

To find the potentials, we substitute the (k, ω) which satisfies the dispersion, and solve for the coefficients A_0 through A_{2N+1}.

3 Numerical examples of dispersion relations

This section will be devoted to numerical examples for the dispersion relations discussed in the previous section, along with several illustrative examples of the potential as a function of depth into the material. The previous relations describe collective excitations which may arise by any number of mechanisms. All we require is the frequency-dependent dielectric constants of the materials involved. We will study an example of metal slabs separated by fixed dielectric layers and, as before, the entire superlattice surrounded by vacuum. The metal (material A) is assumed to have $\epsilon_{\mathrm{A}}(\omega) = 1 - \frac{\omega_p^2}{\omega^2}$, with $\omega_p = 15$ eV (appropriate for Al [27]). Initially we take the fixed dielectric layers (material B) to be vacuum ($\epsilon_{\mathrm{B}} = 1$).

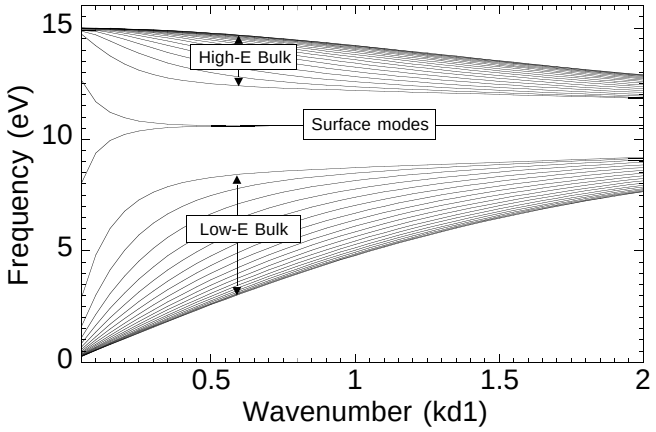

Fig. 2. Dispersion curves for a superlattice ($N = 40$) consisting of films of aluminum separated by vacuum. The plot gives frequency ω *vs.* wavenumber kd_1, with $kd_2 = 0.5kd_1$.

Fixing the thicknesses of the layers to be $d_1 = 2d_2 = 1$, the wavevectors can be swept, finding all corresponding $\epsilon_{\mathrm{A}}(\omega)$ values which satisfy the dispersion relation. These values can then be translated into ω using the equation for $\epsilon_{\mathrm{A}}(\omega)$.

Figure 2 shows the dispersion curves for a superlattice consisting of 20 layers of aluminum separated by vacuum ($N = 40$). They are given as plots of frequency ω *vs.* wavenumber kd_1. For each wavelength, there are 40 corresponding frequency modes possible, two for each active (frequency-dependent) layer present in the superlattice. Three distinct mode groupings are apparent. This is all consistent with previous work done on finite superlattices. The boundaries of these groupings are consistent with those found for semi-infinite superlattices with the same parameters [16]. In essence, the finite case has merely broken up the continuous band of states found in the semi-infinite case into discrete modes.

Each of the modes has a unique electric potential profile $\Phi(z)$, which contains the signature characteristics of its group. We take A_0 to be unity and pairs of known kd_1 and ω which satisfy the dispersion relation. With these, we can calculate the rest of the coefficients A_i in terms of A_0 and then calculate particular $\Phi(z)$.

In Figure 3, plots (a) and (b) show electrostatic potential $\Phi(z)$ *vs.* depth into the structure for the surface modes of a superlattice consisting of aluminum active layers separated by vacuum spacers ($kd_1 = 2kd_2 = 1$). Plot (a) shows the odd surface mode ($\omega = 10.6067$) and (b) the even surface mode ($\omega = 10.6065$). These modes localize on the two outer boundaries of the superlattice and are labeled according to their symmetry, one odd and one even. For large kd_1 they have frequencies that are nearly independent of wavelength, as seen in Figure 2. For long wavelengths (small k) the two modes split apart and the odd surface mode merges with the high-energy bulk band and the even with the low-energy bulk band.

All the modes are, in fact, made up of combinations of single-film-contained surface modes. If one reduces the superlattice to a single film, two modes exist, both being

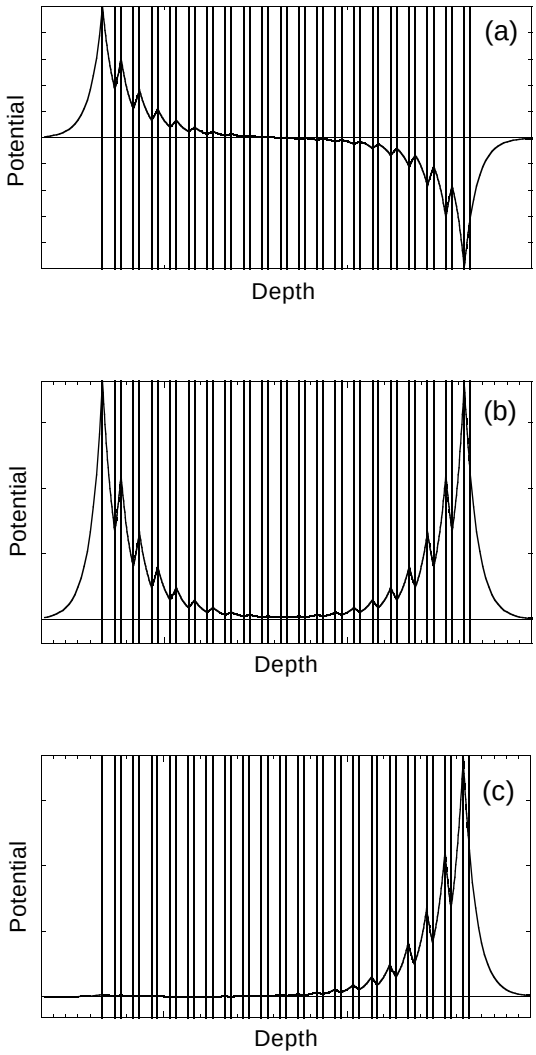

Fig. 3. Plots (a) and (b) show electrostatic potential $\Phi(z)$ *vs.* depth into the structure for a superlattice consisting of aluminum films separated and surrounded by vacuum ($kd_1 = 1.0$, $kd_2 = 0.5kd_1$). Plot (a) shows the odd surface mode ($\omega = 10.6067$ eV) and plot (b) the even ($\omega = 10.6065$ eV). Plot (c) shows the only even surface mode ($\omega = 10.6065$ eV) of the same superlattice with a perturbation of the spacer dielectric to $\epsilon_B = 1.01$. The odd surface mode (not shown) localizes to the other surface.

surface modes since there are no bulk interfaces (and we have explicitly ignored bulk excitations of the individual films). With each frequency-dependent layer added, a pair of high and low energy bulk modes form.

4 Perturbations in layer thickness

4.1 Discussion

In general, the surface modes of a finite superlattice are extremely sensitive to changes in the symmetry of the structure [17]. The greater the number of constituents in the superlattice, the greater the sensitivity [17]. For instance, if the dielectric ϵ_B is changed even by one percent for the superlattice in the previous example, the surface modes dramatically localize their electric potential to one surface of the superlattice. This is a symmetry perturbation since, due to the bi-layer structure, an active layer couples to vacuum on one side while a spacer couples on the other. In Figure 3, plot (c) shows the electrostatic potential *vs.* depth for the *even* surface mode of a superlattice composed of aluminum active layers separated by perturbed spacers ($\epsilon_B = 1.01$, $kd_1 = 2kd_2 = 1$, $\omega = 10.6065$ eV, $N = 40$). Notice the large localization of electric potential without a noticeable change in energy. The odd-symmetry surface mode also localizes, but on the the opposite surface (for brevity, only one of the localized modes is shown in the figure). The bulk modes are insensitive to the offset in the spacer dielectric. In the semi-infinite case, the surface modes show sensitivity by only existing when $d_2 < d_1$ [16].

One might assume that a perturbation of one layer's thickness would cause the same localization of the surface waves within a finite superlattice. This would follow from the known sensitivity of the surface modes of a finite superlattice to the overall structure symmetry and the sensitivity of electron wavefunctions for a set of coupled quantum wells to well-thickness variation [26]. However, for our situation, the analogy does not apply. For layer expansions of either material, no substantial changes in any of the potential profiles are seen until the offsets are very large.

The reason that thickness variations have little affect on the plasmons stems from the fact that, in the absence of other perturbations, the system must evolve continuously into two uncoupled superlattices in the same symmetry environment as the original structure. These uncoupled structures must obey the same high symmetry requirements as any isolated structure; therefore, any coupling between the two can only influence the *internal* structure of the collective modes rather than the global symmetry. Demonstrating this is the main result of this paper.

We note that the difference between this plasmon evolution and that of the electron wavefunction of a set of coupled quantum wells is due to the manner in which the excitations of the individual components of the structure combine to form the collective excitation. The plasmon modes arise from the coupling of surface waves at the boundaries of the individual films. Even the "bulk" excitations are composed of surface waves in the individual layers. The collective electron wavefunctions for a set of coupled quantum wells arise from the coupling of the wavefunctions for the individual wells. Each of these is an excitation localized near the center of the well. Therefore, though the two cases seem synonymous, the perturbations in well thickness and active-layer thickness are not. The increase in an individual quantum well's thickness increases the size of the region in which the overall wavefunction may localize. The increase in active-layer thickness merely loosens the coupling between surface waves existing on nearby interfaces. We also note that variations in the thicknesses of the *inactive* layers of the superlattice and the barriers separating the quantum wells result in completely analogous evolutions.

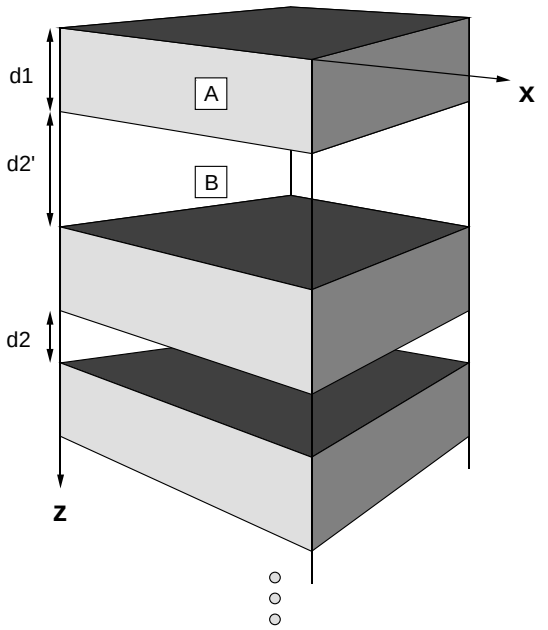

Fig. 4. The physical picture of the superlattice with aluminum active layers (ϵ_A) separated by vacuum spacers with one layer perturbed to a thickness d_2'.

By perturbing a particular material B layer, we effectively create two finite superlattices, separated by a region of ϵ_B, in the case of the spacer layer expansion, and of ϵ_A, in the case of the active layer expansion. Figure 4 shows the physical picture of a spacer layer perturbation, the thickness of that layer changing to d_2'. With $d_2' = d_2$, the superlattices couple "perfectly". As the thickness offset is increased, they begin to behave more and more like two separate superlattices. This is the evolution mentioned earlier. Each superlattice has the same electrostatic potential modes as it would if it were uncoupled, with slight coupling effects from the other superlattice. Thus, how many modes exist in each of the now two superlattices depends upon where the original superlattice was split.

4.2 Dispersions, potential profiles, and "anti-crossings"

The following is a description of numerical dispersion examples followed by a discussion of their qualities. Figure 5 shows plots of dispersion curves (ω *vs.* k) for thickness perturbations. Plots (a) and (b) show dispersions for expansions of the second and tenth, respectively, material B layers from the outside boundary of the superlattice. These correspond to the 4th and 20th layers, with an active layer being counted as the "1st" layer. The superlattices have parameters $N = 40$, $kd_1 = 2kd_2$, $kd_2' = 5kd_1$, with aluminum active layers separated by vacuum. Plot (c) shows the dispersion for a superlattice with the third active layer from the outside boundary expanded to $5kd_1$. This corresponds to the 5th layer, with an active layer being counted as the "1st" layer. Once again, the superlattice has parameters $N = 40$, $kd_1 = 2kd_2$, with aluminum active layers separated by vacuum.

In Figure 5, we effectively plotted dispersion curves for *systems* of superlattices which consisted of two superlattices separated by vacuum, in plots (a) and (b), and by ϵ_A, in plot (c). In plot (a), one superlattice, the "split-off", was an $N = 4$ superlattice, with two metal layers. The other, the "main", was an $N = 36$ superlattice, with 18 metal layers. If the two were completely uncoupled, *i.e.* at very large separation, then the split-off would have two surface modes and two bulk modes, one high and one low energy. The main structure would have two surface modes and 34 bulk modes, 17 high and 17 low energy. When coupled, the structures maintain the same numbers and types of modes. This is why in the dispersion of the system has the effect of superimposing the two superlattices' dispersions on top of one another. It is still true that there are no intersections between any of the modes, thus, there are still 40 unique excitation frequencies for every possible wavelength.

Plots (b) and (c) of Figure 5 show similar characteristics. Plot (c), however, has a slightly different division of the plasmon modes. Since the perturbation is of an active (metal) layer, the *system* consists of two superlattices coupling *via* that active layer. Thus, the uncoupled equivalent is two superlattices with metallic semi-infinite substrates. With the third active layer expanded (and vacuum spacers), the two superlattices are an $N = 4$ and an $N = 34$. Each will have the usual numbers of modes, with an additional mode contributed by the active substrate.

The active layer perturbation has an additional effect of localizing the surface modes of the uncoupled superlattices. This is in the same fashion as the spacer layer dielectric perturbation discussed earlier. The bulk modes will remain fairly unaffected, and will look the same as the bulk modes in spacer-layer-perturbed systems.

If we look carefully at the dispersion curves shown in Figure 5, plot (a), it almost appears as if the split-off surface mode dispersion curves cross or touch the surrounding bulk modes on their way to merging with the main superlattice's surface modes at short wavelengths (see arrows on plot). This is actually an interesting point in the dispersion. It is more apparent in Figure 6 which shows the dispersions (ω *vs.* k) for two completely uncoupled superlattices, one an $N = 4$ and one an $N = 36$, superimposed on one another. Both superlattices are assumed to have $kd_2 = 0.5kd_1$ and be composed of aluminum active layers separated by vacuum. The dotted lines are the dispersion curves for the $N = 36$ superlattice and the solid lines are for the $N = 4$. We can see that the dispersion curves actually cross one another in the completely uncoupled system.

These crossings are four "anti-crossings" in the coupled system which occur at two values of kd_1, roughly $kd_1 = 0.07$ and $kd_1 = 0.517$. The dispersion curves approach one another, but do not cross. However, the electrostatic potentials associated with the modes switch. By this we mean that at wavelengths longer than that of the anti-crossing value the potentials behave in one manner, and for wavelengths shorter they behave another. This is quite interesting since in no other situation has there been any

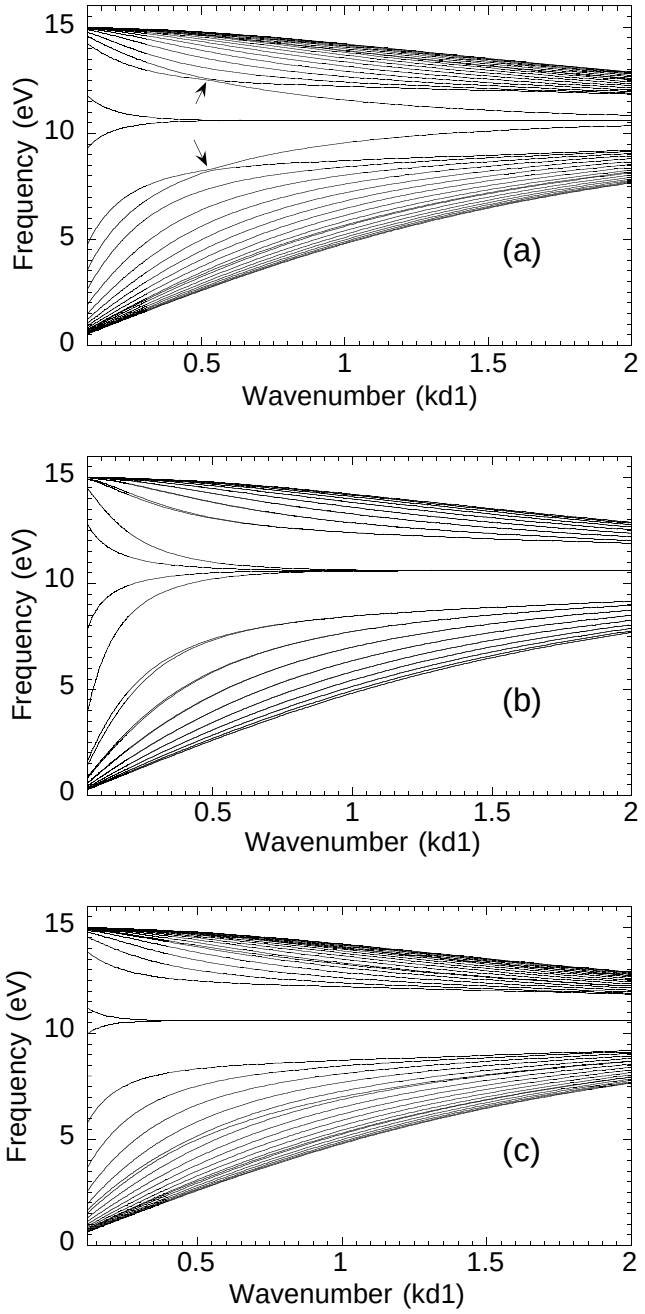

Fig. 5. Dispersion plots of frequency ω *vs.* wavenumber kd_1. All plots have parameters $kd_2 = 0.5kd_1$, $\epsilon_B = 1$, and $N = 40$. Plots (a) and (b) show the dispersion curves for superlattices with their second and tenth, respectively, material B layers perturbed in thickness to $5kd_1$. The arrows in plot (a) accent the anti-crossings in the dispersion. Plot (c) shows the dispersion for a superlattice with its third active layer perturbed in thickness to $5kd_1$.

significant change in a particular potential profile with a change in wavelength.

Figure 7 shows potential profiles at two different kd_1 values for the even split-off surface mode and the neighboring low-energy bulk mode. Plots (a) and (b) show the two modes at $kd_1 = 0.7$, with $\omega = 8.491$ eV and $\omega = 8.885$ eV, respectively. Following the dispersion curves

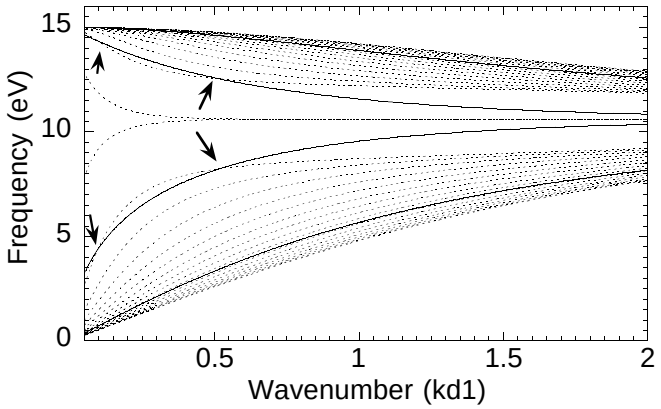

Fig. 6. Dispersion curves for uncoupled $N = 4$ (solid lines) and $N = 36$ (dashed lines) superlattices superimposed on one another. Both superlattices consist of aluminum active layers separated and surrounded by vacuum, with $kd_2 = 0.5kd_1$. The four arrows point to the four crossings that become anti-crossings when when the superlattices are coupled.

down to $kd_1 = 0.4$, plots (c) and (d) show the two modes in the same order, with $\omega = 7.564$ eV and $\omega = 7.952$ eV, respectively. We can see that the mode in plot (a) is a fairly well-defined low-energy bulk mode at $kd_1 = 0.7$. However, at $kd_1 = 0.4$, below the anti-crossing, this mode behaves like a surface mode in the separated superlattice (plot (c)). The same switch takes place between the pairs of modes involved in the other anti-crossings.

It is less obvious, but the same anti-crossing behavior appears in plot (c) of Figure 5. Once again this is merely due to the affect of superimposing the uncoupled dispersions on top of one another. As the separate superlattices begin to couple, the points where their uncoupled dispersions would cross become the anti-crossings. In fact, the only situation in which the anti-crossings do not occur is the case of two identical superlattices coupling. They may couple *via* vacuum as shown in plot (b) of Figure 5, or *via* an active region. In either case, the uncoupled dispersions are exactly the same and therefore as the superlattices couple slightly, the modes merely split into parallel pairs, never crossing.

4.3 Atomic-to-molecular analogy

An interesting comparison arises between the interaction of two finite superlattices and two atoms. As the superlattices approach one another, the electromagnetic coupling effects cause changes in the frequencies of the plasmon excitation modes. In the example of two identical superlattices, the pairs of like plasmon excitation energies split. This is analogous to two identical atoms splitting their degenerate energy levels as they couple due to wavefunction overlap. We note that a similar analogy is often made between the coupling of like atoms and the coupling of electron wavefunctions for identical quantum wells.

We saw in Figure 5, plot (b), the plasmon dispersion for two identical coupled superlattices containing 20 layers, 10 of aluminum and 10 vacuum, with $kd_1 = 2kd_2$ and

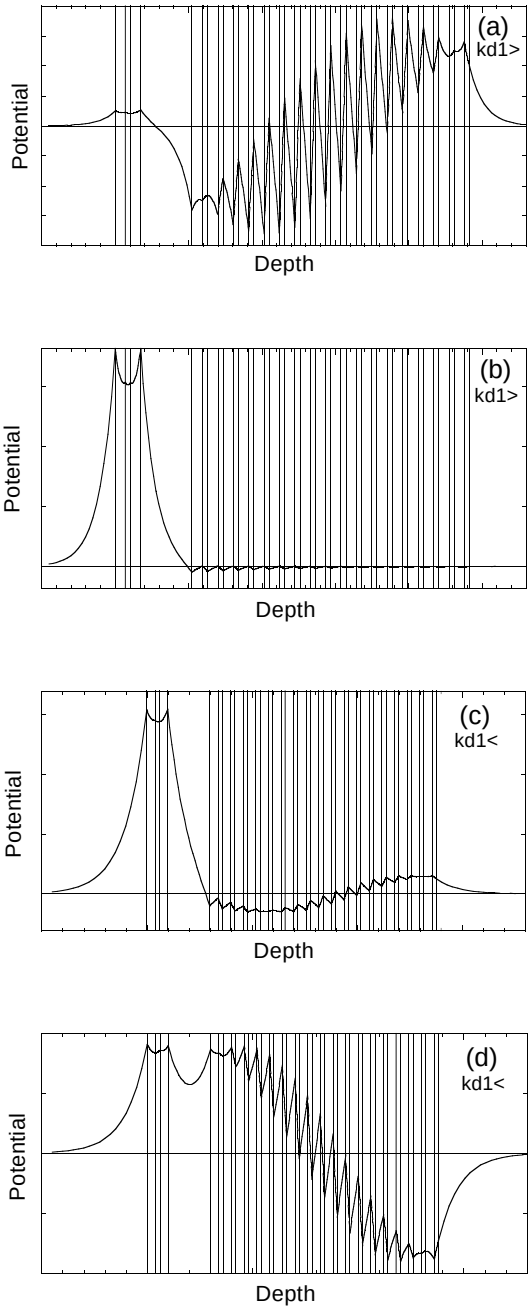

Fig. 7. Plots of electric potential *vs.* depth into the superlattice at two different kd_1 values for the even split-off surface mode and the neighboring low-energy bulk mode. Plots (a) and (b) show the two modes at $kd_1 = 0.7$, with $\omega = 8.491$ eV and $\omega = 8.885$ eV, respectively. Following the dispersion curves down to $kd_1 = 0.4$, plots (c) and (d) show the two modes in the same order, with $\omega = 7.564$ eV and $\omega = 7.952$ eV, respectively.

$kd_2' = 5kd1$. At this separation distance, we can see the splitting of the dispersion curves in pairs. As the separation becomes smaller, the curves smoothly approach those shown for the original, unperturbed superlattice.

Figure 8 shows a plot of frequency (ω) *vs.* separation distance (kd_2') between the two identical superlattices. kd_1 is fixed at 2.0, $kd_2 = 0.5kd_1$, $\epsilon_B = 1$, and kd_2' values are

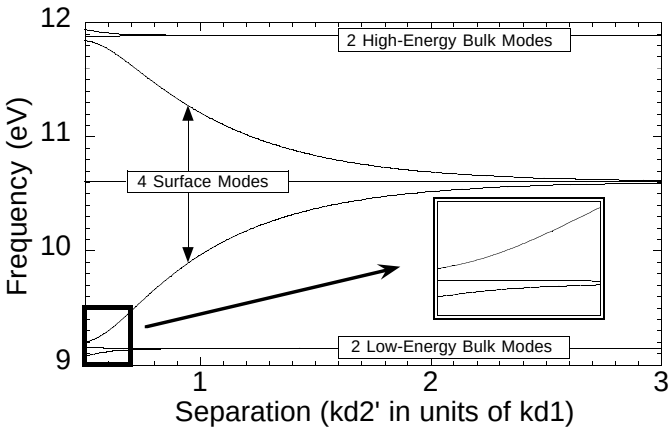

Fig. 8. Plot of frequency ω *vs.* separation kd_2' (in units of kd_1) between two identical superlattices. The superlattices are assumed to be $kd_1 = 2.0$, $kd_2 = 0.5kd_1$, $N = 20$, with aluminum active layers and vacuum spacers. For each kd_2' value, the frequencies of the odd and even surface modes (4) are calculated along with the frequencies of the two pairs of neighboring bulk modes (2 high and 2 low energy).

swept through in units of kd_1. For each kd_2' value, the frequencies of the even and odd surface modes, the two neighboring high-energy bulk modes, and the two neighboring low-energy bulk modes are plotted. At a large separation, the surface modes and the two pairs of bulk modes are nearly degenerate.

As the superlattices approach one another the electromagnetic coupling increases, causing the potential profiles of the plasmon modes to assume odd-even parities. This is similar to bonding/anti-bonding pairs in the molecular orbital case.

Notice that one even and one odd surface mode dramatically change their energy as the separation decreases, the even merging with the low-energy bulk band and the odd with the high-energy bulk band. The other surface modes remain at the same (or nearly the same) energy. Similar, but less dramatic, behavior appears in the bulk mode pairs, with one staying fairly constant and the other changing.

4.4 Dual perturbations

It is interesting to study the effects of combined perturbations. With the layer thickness perturbation in place, we can add in the spacer dielectric perturbation. Figure 9 shows the surface modes of the coupled split-off ($N = 4$) and main ($N = 36$) superlattices with $kd_1 = 2.0$, $kd_2' = 5kd_1$, $kd_2 = 0.5kd_1$, and a perturbed spacer dielectric of $\epsilon_B = 1.01$. Plot (a) shows the even split-off surface mode ($\omega = 10.350$ eV). Plot (b) shows the even main surface mode ($\omega = 10.580$ eV). Plot (c) shows the odd main surface mode ($\omega = 10.583$ eV). Plot (d) shows the odd split-off surface mode ($\omega = 10.829$ eV). The surface modes of the main localize just as they would if the two superlattices were uncoupled. The split-off surface modes are insensitive to the perturbation since their potentials

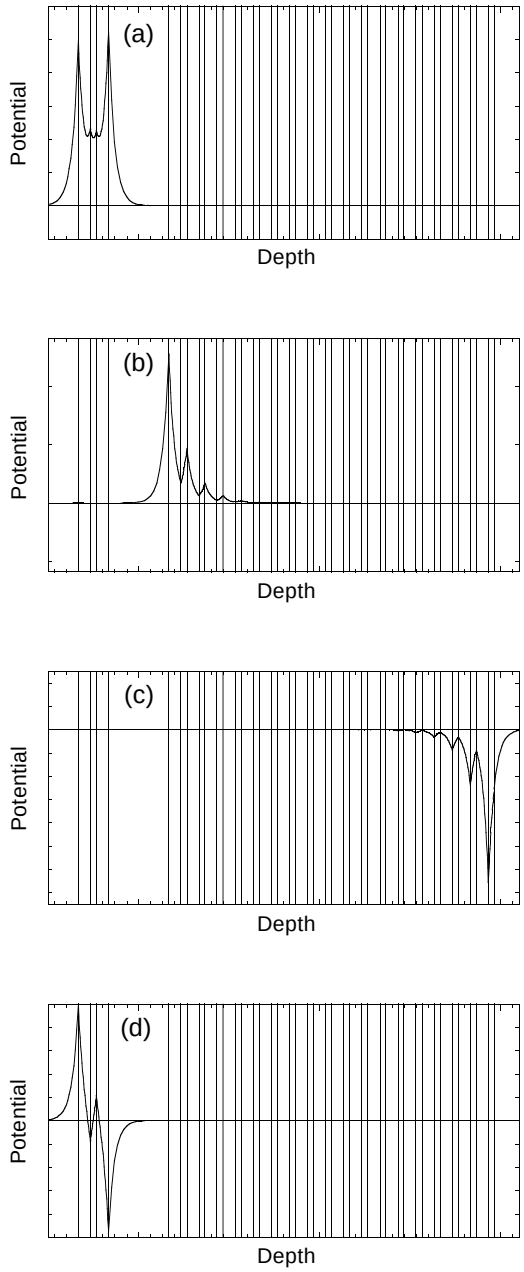

Fig. 9. Layer thickness and spacer dielectric perturbation plots of electrostatic potential *vs.* depth into the superlattice ($kd_1 = 2.0$, $kd_2 = 0.5kd_1$, $kd_2' = 5kd_1$, $\epsilon_{\rm B} = 1.01$, and $N = 40$, with the second material B layer expanded). Plot (a) shows an even split-off surface mode ($\omega = 10.350$ eV). Plot (b) shows a localized even main surface mode ($\omega = 10.580$ eV). Plot (c) shows a localized odd main surface mode ($\omega = 10.583$ eV). Plot (d) shows an odd split-off surface mode ($\omega = 10.829$ eV).

drop off well before the interface on the opposing side of the perturbed layer.

5 Summary

In this paper we presented a study of plasmon excitations within a finite superlattice, including the effects of thickness variation. Numerical examples were given, showing dispersion curves for a superlattice made up of 20 layers of aluminum alternating with 20 layers vacuum. We chose particular modes from the dispersion to display the different potential profile characteristics possible within a finite superlattice. With this existing knowledge, our goal was then to explore the effects of thickness variations on the plasmon modes of the superlattice.

As mentioned above, the surface plasmon modes are very sensitive to the value of the dielectric constant of the static layers (*i.e.* to the overall symmetry of the structure), while at the same time the surface modes are nearly insensitive to variations in the thickness of layers within the superlattice. The overall structure of the plasmon modes is insensitive to deviations in the thicknesses of either the free-charge carrying layers or the dielectric spacer layers, in contrast to the case of electrons in quantum wells, where the wavefunction morphology depends upon whether the thickness of the well or the barrier is changed. The analogy between the quantum wells and the superlattice is strict if only barrier thickness deviations are considered.

When the thickness variation becomes very large, the system evolves smoothly into that of two uncoupled superlattices. This behavior is similar to that of the wavefunctions for atomic orbitals as two distant atoms are brought together. The introduction of long-range coupling splits the degenerate energy levels (with the magnitude of the splitting dependent upon the inter-nuclear distance), and the wavefunctions evolve into molecular orbitals. In the present case, the dispersions show splitting inversely proportional to the layer-thickness variation, and the potentials evolve into superlattice modes.

This work was supported by an award from the Research Cooporation, and by the BFR at WWU support for undergraduate research.

References

1. R.E. Camley, T.S. Raman, D.L. Mills, Phys. Rev. B **27**, 261 (1983).
2. M. Grimsdites, M.R. Kahn, A. Kenney, I.K. Schuller, Phys. Rev. Lett. B **51**, 498 (1983).
3. P. Grunberg, K. Mika, Phys. Rev. B **27**, 2995 (1983).
4. R.L. Stamps, R.E. Camley, Phys. Rev. B **54**, 15200 (1996).
5. M. Hammouchi, E.H. El Boudouti, A. Nougaoui, B. Djafari-Rouhani, M.L.H. Lahlaouti, A. Akjouj, L. Dobrzynski, Phys. Rev. B **59**, 1999 (1999).
6. W. Chen, Y. Lu, H.J. Marris, G. Xiao, Phys. Rev. B **50**, 14506 (1994).
7. H.J. Trodhal, P.V. Santos, G.V.M. Williams, A. Bittar, Phys. Rev. B **40**, 8577 (1989).
8. B.A. Auld, G.A. Bempre, G. Gerrmann, Electron Lett. **13**, 525 (1977).
9. J. Mendialdua, A. Rodriguez, M. Move, A. Akjouj, L. Dobrzynski, Phys. Rev. B **50**, 14605 (1994).
10. B.L. Johnson, R.E. Camley, Phys. Rev. B **43**, 6554 (1991).
11. R.L. Stamps, R.E. Camley, Phys. Rev. B **40**, 596 (1989).

12. B. Lamprecht, J.R. Krenn, G. Schider, H. Ditlbacher, M. Salerno, N. Felidj, A. Leitner, F.R. Aussenegg, J.C. Weeber, Appl. Phys. Lett. **79**, 51 (2001).
13. K. Golden, G. Kalman, L. Miao, R. Snapp, Phys. Rev. B **55**, 16349 (1997).
14. D. Lu, K.I. Golden, G. Kalman, P. Wyns, L. Miao, X-L. Shi, Phys. Rev. B **54**, 11457 (1996).
15. K. Golden, G. Kalman, L. Miao, R. Snapp, Phys. Rev. B **57**, 9883 (1998).
16. R.E. Camley, D.L. Mills, Phys. Rev. B **29**, 1695 (1984).
17. B.L. Johnson, J.T. Weiler, R.E. Camley, Phys. Rev. B **32**, 6544 (1985).
18. S. Das Sarma, E.H. Hwang, Phys. Rev. Lett. **81**, 4216 (1998).
19. L. Wendler, T. Kraft, Phys. Rev. B **60**, 16603 (1999).
20. N.-H. Kwong, M. Bonitz, Phys. Rev. Lett. **84**, 1768 (2000).
21. G.F. Guiliani, J.J. Quinn, Phys. Rev. Lett. **51**, 919 (1983).
22. D. Olego, A. Pinzuk, A.C. Gossard, W. Wiegmann, Phys. Rev. B **25**, 7867 (1982).
23. R.L. Stamps, B.L. Johnson, R.E. Camley, Phys. Rev. B **43**, 3626 (1991).
24. B.L. Johnson, R.E. Camley, Solid State Comm. **59**, 595 (1986).
25. W.L. Bloss, Phys. Rev. B **44**, 1105 (1991-I).
26. R.K. Littleton, R.E. Camley, J. Appl. Phys. **59**, 2817 (1986).
27. G. Chiarello, V. Formoso, A. Santaniello, E. Colavita, L. Papagno, Phys. Rev. B **62**, 12676 (2000).